Jianzhang Li*, Sven Nebelung, Björn Rath, Markus Tingart and Jörg Eschweiler

A novel combined level set model for automatic MR image segmentation

Abstract: Medical image processing comes along with object segmentation, which is one of the most important tasks in that field. Nevertheless, noise and intensity inhomogeneity in magnetic resonance images challenge the segmentation procedure. The level set method has been widely used in object detection. The flexible integration of energy terms affords the level set method to deal with variable difficulties. In this paper, we introduce a novel combined level set model that mainly cooperates with an edge detector and a local region intensity descriptor. The noise and intensity inhomogeneities are eliminated by the local region intensity descriptor. The edge detector helps the level set model to locate the object boundaries more precisely. The proposed model was validated on synthesized images and magnetic resonance images of in vivo wrist bones. Comparing with the ground truth, the proposed method reached a Dice similarity coefficient of > 0.99 on all image tests, while the compared segmentation approaches failed the segmentations. The presented combined level set model can be used for the object segmentation in magnetic resonance images.

Keywords: level set method, MRI, segmentation, intensity inhomogeneity

https://doi.org/10.1515/cdbme-2020-3006

1 Introduction

In the medical field, decomposition of an image is challenging due to images' poor quality, e.g. occlusion, low signal, and contrast, or noises. The Level Set Method (LSM) has become a popular technique in recent years [1, 2]. Two main classes represent the typical LSM, which are edge-based [2, 3] and region-based models [4–6].

Edge-based models use edge information to detect object boundaries. This type of model has been found very sensitive to image noise [1]. Region-based models detect the object by calculating intensity in the foreground and background on the image domain. In magnetic resonance (MR) images, the intensity inhomogeneity occurs from a non-uniform magnetic field due to a variety of reasons [7]. Particularly, any intensity inhomogeneity may lead to erroneous segmentation outcomes when the object has a similar intensity as the background. Two similar local region descriptors were proposed to overcome such problems [5][6]. Pixels inside the selected region are calculated based on local intensity similarity to avoid inhomogeneity on global image domain.

By adding different energy functionals, the LSM can deal with variable image processing scenes. In this paper, we propose a combined level set model for object segmentation in MR images of in vivo wrist bones. Our model consists of an edge detector and a local intensity descriptor for the segmentation purpose, and a regularization term to maintain evolving stability. Experimental results on synthesized images and MR images are presented to demonstrate the power and opportunities of the proposed combined level set model. Our study aimed to provide an automatic MR image segmentation approach with a high segmentation accuracy compared to existing methods.

2 Material and Method

2.1 LSM

Given a moving curve $\mathcal{C}$, the core of the LSM is to implicitly describe $\mathcal{C}$ by the zero level of a higher dimensional function $\phi: \Omega \to \Re$ as: $\mathcal{C}(t) = \{x \in \Omega \mid \phi(x,t) = 0\}$. The evolving equation can be expressed in the following partial differential equation:

$$\frac{\partial \phi}{\partial t} = \mathcal{F}|\nabla \phi|, \tag{1}$$

***Corresponding author: Jianzhang Li:** Department of Orthopaedic Surgery, RWTH Aachen University Clinic, Pauwelsstraße 30, 52074, Aachen, Germany. E-mail: jli@ukaachen.de

Sven Nebelung: Institute of Diagnostic and Interventional Radiology, University Hospital Düsseldorf, Düsseldorf, Germany.

Björn Rath: Department of Orthopaedic Surgery, Klinikum Wels-Grieskirchen, Wels, Austria.

Markus Tingart, Jörg Eschweiler: Department of Orthopaedic Surgery, RWTH Aachen University Clinic, Aachen, Germany.

where ∇ is the gradient operator, and $\mathcal{F}$ the speed function that controls the motion of the contour. By choosing the function $\mathcal{F}$, the LSM can reach different segmentation goals. A typical choice is to define the $\mathcal{F}$ as a boundary detector [3] or a global intensity descriptor [4].

2.2 Edge detection energy term

Edge information is widely applied for segmentation methods [2, 3, 8]. Here, we utilize the edge detection energy term to guide the evolving curve. The image $I: \Omega \to \Re$ is a given grey level image on the domain Ω, we define a function g as an edge detector by:

$$\boldsymbol{g} = \frac{\mathbf{1}}{\mathbf{1}+|\nabla \boldsymbol{G}_{\sigma} * \boldsymbol{I}|^2}, \tag{2}$$

where $G_\sigma * I$ is the convolved I by a Gaussian kernel G_σ with a standard deviation σ. For a level set function $\phi: \Omega \to \Re$, we define the edge detection energy term $\mathcal{E}_{Edge}(\phi)$ by:

$$\boldsymbol{\mathcal{E}_{Edge}(\phi)} = \boldsymbol{\mu} \int_{\boldsymbol{\Omega}} \boldsymbol{g\delta(\phi)|\nabla\phi|}\, \boldsymbol{dx}, \tag{3}$$

where $\mu > 0$, $\delta(x)$ is the Dirac delta function.

2.3 The local intensity energy term

To enhance the segmentation against image noise and intensity inhomogeneity in MR images, a Gaussian distribution kernel works as the local region descriptor. Comparing with [5], the Gaussian distribution kernel has such property that weights the intensities around a small interested area. For a given point $x \in \Omega$, we define the local intensity energy term as:

$$\boldsymbol{\mathcal{E}_{Local}(\phi, f_1(x), f_2(x))} = \sum_{\boldsymbol{i}=\mathbf{1}}^{\mathbf{2}} \boldsymbol{\lambda_i} \int_{\boldsymbol{\Omega}} \Big(\boldsymbol{K_\xi(x-y)|I(y) - f_i(x)|^2 L_i(\phi(y))} \Big)\, \boldsymbol{dy}\Big)\, \boldsymbol{dx}, \tag{4}$$

where $\lambda_i > 0$, $L_1(\phi) = H(\phi)$, $L_2(\phi) = 1 - H(\phi)$, $H(x)$ is the Heaviside function, K_ξ the Gaussian kernel with a scale parameter $\xi > 0$, and $f_1(x)$, $f_2(x)$ approximate intensities in a neighbourhood of x inside and outside the contour $\mathcal{C}$. The $f_i(x)$ is computed using the Euler-Lagrange equations:

$$\boldsymbol{f_i(x)} = \frac{\boldsymbol{K_\xi(x) * \big(L_i(\phi(x)) I(x)\big)}}{\boldsymbol{K_\xi(x) * \big(L_i(\phi(x))\big)}}, \boldsymbol{i = 1, 2}. \tag{5}$$

2.4 Regularization energy term

During the evolving procedure, the conventional LSM has been trapped by reinitialization for a long time. Li et al. introduced a regularization term to maintain the level set function as the signed distance function [8]. We apply the regularization term against the reinitialization problem as:

$$\boldsymbol{\mathcal{E}_{Reg}(\phi)} = \boldsymbol{\alpha} \int_{\boldsymbol{\Omega}} \frac{\mathbf{1}}{\mathbf{2}} (|\boldsymbol{\nabla\phi(x)}| - \mathbf{1})^{\mathbf{2}}\, \boldsymbol{dx}, \tag{6}$$

where $\alpha > 0$ is the coefficient.

2.5 Combined level set model and numerical implementation

As described above, the proposed combined level set model in this work is defined as:

$$\boldsymbol{\mathcal{F}_{Combined}} = \boldsymbol{\mathcal{E}_{Reg}} + \boldsymbol{\mathcal{E}_{Edge}} + \boldsymbol{\mathcal{E}_{Local}}. \tag{7}$$

After replacing energy terms, we can obtain the speed energy functional $\mathcal{F}$ as:

$$\boldsymbol{\mathcal{F}_{Combined}} = \boldsymbol{\alpha} \int_{\boldsymbol{\Omega}} \frac{\mathbf{1}}{\mathbf{2}} (|\boldsymbol{\nabla\phi(x)}| - \mathbf{1})^{\mathbf{2}}\, \boldsymbol{dx} + \boldsymbol{\mu} \int_{\boldsymbol{\Omega}} \boldsymbol{g\delta(\phi)|\nabla\phi|}\, \boldsymbol{dx} + \sum_{\boldsymbol{i}=\mathbf{1}}^{\mathbf{2}} \boldsymbol{\lambda_i} \int_{\boldsymbol{\Omega}} \Big(\int_{\boldsymbol{\Omega}} \Big(\boldsymbol{K_\xi(x-y)|I(y) - f_i(x)|^2 L_i(\phi)} \Big)\, \boldsymbol{dy} \Big)\, \boldsymbol{dx}. \tag{8}$$

In practical implementation, the Heaviside function H and the Dirac delta function δ are approximated by following smoothed functions H_ϵ and δ_ϵ respectively, defined as:

$$\boldsymbol{H_\epsilon} = \begin{cases} \frac{\mathbf{1}}{\mathbf{2}} \Big(\mathbf{1} + \frac{\boldsymbol{x}}{\boldsymbol{\epsilon}} + \frac{\mathbf{1}}{\boldsymbol{\pi}} \boldsymbol{sin} \Big(\frac{\boldsymbol{\pi x}}{\boldsymbol{\epsilon}} \Big) \Big), |\boldsymbol{x}| \le \boldsymbol{\epsilon} \\ \mathbf{1}, \boldsymbol{x} > \boldsymbol{\epsilon} \\ \mathbf{0}, \boldsymbol{x} < -\boldsymbol{\epsilon} \end{cases}, \tag{9}$$

and

$$\boldsymbol{\delta_\epsilon} = \begin{cases} \frac{\mathbf{1}}{\mathbf{2}\boldsymbol{\epsilon}} \Big(\mathbf{1} + \boldsymbol{cos} \big(\frac{\boldsymbol{\pi x}}{\boldsymbol{\epsilon}} \big) \Big), |\boldsymbol{x}| \le \boldsymbol{\epsilon} \\ \mathbf{0}, |\boldsymbol{x}| > \boldsymbol{\epsilon}, \end{cases}, \tag{10}$$

where ϵ is the coefficient and usually set to the value of 1.5. The minimization of $\mathcal{F}_{Combined}$ concerning to ϕ can be attained using standard gradient descent method:

$$\frac{\boldsymbol{\partial\phi}}{\boldsymbol{\partial t}} = -\frac{\boldsymbol{\partial \mathcal{F}}}{\boldsymbol{\partial\phi}}, \tag{11}$$

where $\partial\mathcal{F}/\partial\phi$ is the Gâteaux derivative of the $\mathcal{F}$. Hence, the corresponding gradient flow equation is expressed as:

$$\frac{\boldsymbol{\partial\phi}}{\boldsymbol{\partial t}} = -\boldsymbol{\alpha} \Big(\boldsymbol{\nabla^2\phi - div} \Big(\frac{\boldsymbol{\nabla\phi}}{\boldsymbol{|\nabla\phi|}} \Big) \Big) - \boldsymbol{\mu\delta_\epsilon(\phi) div} \Big(\boldsymbol{g} \frac{\boldsymbol{\nabla\phi}}{\boldsymbol{|\nabla\phi|}} \Big) + \boldsymbol{\delta_\epsilon(\phi)} (\boldsymbol{\lambda_1 e_1 - \lambda_2 e_2}), \tag{12}$$

where $div(\cdot)$ is the divergence operator, e_i is defined as:

$$\boldsymbol{e_i} = \int_{\boldsymbol{\Omega}} \big(\boldsymbol{K_\xi(y-x)|I(x) - f_i(y)|^2} \big) \boldsymbol{dy}. \tag{13}$$

We set the initial level set function with a rectangle form as:

$$\boldsymbol{\phi_0(x)} = \begin{cases} -\boldsymbol{c_0}, \boldsymbol{x} \in \boldsymbol{inside} \\ \boldsymbol{c_0}, \boldsymbol{otherwise} \end{cases}, \tag{14}$$

where $c_0 = 2$ in our approach. The overall algorithm is summarized in Algorithm 1.

We applied the proposed method on synthesized images and MR images of the capitate. The MR images were acquired in vivo using the high-resolution 3D-WATSc (water selective cartilage scans) sequence on a clinical 3T MRI scanner

(Achieva, Philips Healthcare, Best, The Netherlands). The synthesized image was a manually generated heart shape binary image with added Gaussian noise and Salt-and-pepper noise in MATLAB (Version R2019a; The MathWorks, Inc.). All images have not been preprocessed except cropped to a pixel size of 500×500. To comprehensively evaluate the performance of the combined level set model in segmentation tasks, we compared the results of multi-threshold method and edge-based method DRLSE in [8]. Manual segmentation performed by a radiologist with eight years of experience in musculoskeletal radiology provided the ground truth. The curve evolution and results evaluation were conducted in MATLAB.

Algorithm 1

Input: $\phi_0, \alpha, \mu, \rho, \lambda_1, \lambda_2$, iteration number n
Output: ϕ
1. Initialization: $\phi \leftarrow \phi_0$;
2. **for** $i = 0 \rightarrow n$ **do**
3. update g, f_1, f_2 using Eqs. (2) and (7);
4. $\phi^{i+1} \leftarrow \phi^i + \Delta t \Delta \phi^i$;
5. **end for**

3 Results

The parameters of the combined level set model were assigned as $\alpha = 0.2$, $\mu = 0.001 \times 256^2$, $\rho = -3$, $\lambda_1 = \lambda_2 = 1$. The iteration number of all LSM based approaches was empirically set at a position where there was no further evolution of the method we put forward. The segmentation results are shown in figure 1. For evaluating the accuracy, we utilized the Dice similarity coefficient between obtained contours and ground truth. A higher value of the coefficient means better performance. For a given set of regions $\mathcal{G}$ representing the ground truth and $\mathcal{S}$ representing the segmentation, the similarity between $\mathcal{G}$ and $\mathcal{S}$ is expressed as:

$$\boldsymbol{Dice}(\mathcal{G}, \mathcal{S}) = \frac{2 \times |\mathcal{G} \cap \mathcal{S}|}{|\mathcal{G}| + |\mathcal{S}|}. \quad (15)$$

3.1 Synthesized image tests

The dark heart shape area was the object to be segmented. The proposed approach was compared with the DRLSE method. The segmentation with the proposed model stopped after 390 iterations. With the help of local intensity energy term, the evolving curve could merge and analyse the intensities within a small area around interest front points, which provided the correct contour. Nevertheless, as showed in figure 1, the segmentation of the DRLSE method failed after the same iterations due to the massive artificial noises, which blurred the actual object boundaries. The Dice coefficient is listed in Table 1.

Table 1: Dice similarity coefficient on image tests

Test group	Low threshold	High threshold	DRLSE method	Proposed method
Synthesized image			0.9699	0.9959
MR image A	0.9313	0.9517	0.7605	0.9932
MR image B	0.9135	0.6477	0.6751	0.9987
MR image C	0.9117	0.7107	0.6438	0.9995

3.2 MR image tests

To illustrate the difficulties in segmenting MR images, the combined level set model was compared with the conventional multi-threshold method and the DRLSE method. The multi-threshold method was conducted in the free, open-source platform ITK-SNAP [9]. The results were then transferred into MATLAB for evaluation.

The choice of the thresholds is challenging since it is either too low leading to an under-segmentation or too high causing an over-segmentation. There were two attempts on setting the thresholds in this section. For MR image A, B and C, the lower value at 16.3%, 7.78% and 18.19% of each maximum image grey value was to make sure the least leakage outside the capitate bone. The higher value at 29.2%, 18.19% and 28.57% of each maximum image grey value was intended to cover all the areas inside the capitate bone. As for two other LSM approaches, we compared the segmentation results of our proposed model with the DRLSE method. The evolving of each model was terminated after 270, 110 and 115 iterations, respectively. As illustrated in figure 1, the multi-threshold method failed on both choices. Our combined level set model converged after 270, 110 and 115 iterations, respectively, and all desired boundaries were fully covered, while the DRLSE method stopped near the initial ϕ_0 due to its sensitivity to the image noise and intensity inhomogeneity.

4 Conclusion

This paper proposed a combined level set model that reinforces the segmentation in MR images. In this proposed method, we integrated the edge-based energy term and local region-based energy term, which provided additional boundary information and suppressed massive noises and intensity inhomogeneity, respectively. Experimental results showed that the proposed combined level set model possesses a much better accuracy with all Dice similarity coefficients > 0.99.

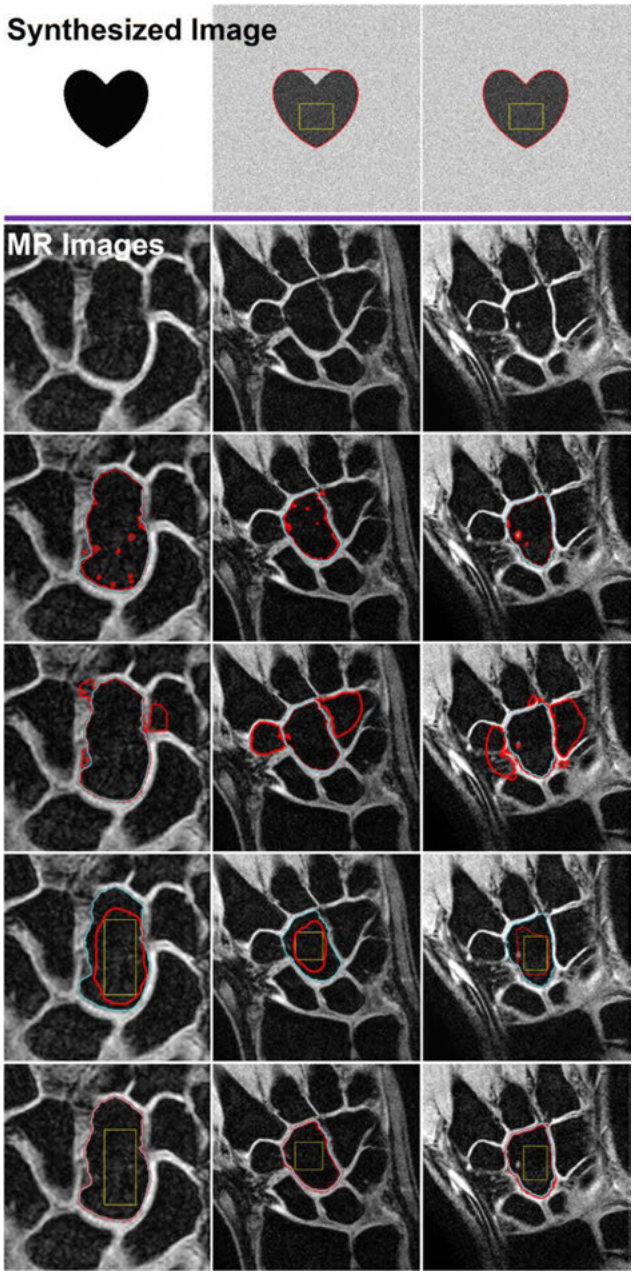

Figure 1: Image test results. **Synthesized Image:** *from left to right:* Original sketch image defined as ground truth; Segmentation of contours by use of the DRLSE method; Segmentation of contours by use of proposed level set model. **MR Images:** *from left to right:* MR image A, B and C. *From up to down:* Original MR image; Segmentation of capitate using the multi-threshold method with lower threshold; Segmentation of multi-threshold method with higher threshold; Segmentation of DRLSE method; Segmentation of the proposed level set model. ***Red line*:** Segmentation contour. ***Yellow line*:** Initial zero level set. ***Cyan line:*** Ground truth.

Author Statement

Research funding: The research was funded by the Deutsche Forschungsgemeinschaft (DFG, German Research Foundation) – ES 442/1-1 and RA 2187/4-1.

Conflict of interest: Authors state no conflict of interest.

Informed consent: Informed consent has been obtained from all individuals included in this study.

Ethical approval: The research related to human use complies with all the relevant national regulations, institutional policies and was performed in accordance with the tenets of the Helsinki Declaration, and has been approved by the authors' institutional review board (EK 171/10).

References

[1] Li C, Huang R, Ding Z, Gatenby JC, Metaxas DN, Gore JC et al. A Level Set Method for Image Segmentation in the Presence of Intensity Inhomogeneities With Application to MRI. IEEE transactions on image processing a publication of the IEEE Signal Processing Society 2011;20(7):2007–16.

[2] Vasilevskiy A, Siddiqi K. Flux maximizing geometric flows. IEEE Trans. Pattern Anal. Machine Intell. 2002;24(12):1565–78.

[3] Caselles V, Kimmel R, Sapiro G. Geodesic Active Contours. Int J Comput Vision 1997;22(1):61–79.

[4] Chan TF, Vese LA. Active contours without edges. IEEE Trans. on Image Process. 2001;10(2):266–77.

[5] Lankton S, Tannenbaum A, Lankton S, Tannenbaum A. Localizing region-based active contours. IEEE transactions on image processing a publication of the IEEE Signal Processing Society 2008;17(11):2029–39.

[6] Li C, Kao C-Y, Gore JC, Ding Z, Gore JC. Minimization of Region-Scalable Fitting Energy for Image Segmentation. IEEE transactions on image processing a publication of the IEEE Signal Processing Society 2008;17(10):1940–9.

[7] Li C, Kao C-Y, Gore JC, Ding Z. Implicit Active Contours Driven by Local Binary Fitting Energy 2007:1–7.

[8] Li C, Xu C, Gui C, Fox MD. Distance Regularized Level Set Evolution and Its Application to Image Segmentation. IEEE transactions on image processing a publication of the IEEE Signal Processing Society 2010;19(12):3243–54.

[9] Yushkevich PA, Piven J, Hazlett HC, Smith RG, Ho S, Gee JC et al. User-guided 3D active contour segmentation of anatomical structures: significantly improved efficiency and reliability. NeuroImage 2006;31(3):1116–28.